Article

Controlling Fast Nucleation and Crystallization of Two New Polyoxoniobates

Joanna Dopta, Dana-Céline Krause, Christian Näther, and Wolfgang Bensch

Cryst. Growth Des., **Just Accepted Manuscript** • DOI: 10.1021/acs.cgd.8b00548 • Publication Date (Web): 08 Jun 2018

Controlling Fast Nucleation and Crystallization of Two New Polyoxoniobates

*Joanna Dopta, Dana-Céline Krause, Christian Näther, Wolfgang Bensch**

Institut für Anorganische Chemie, Christian-Albrechts-Universität Kiel, Max-Eyth-Straße 2, D-24118 Kiel, Germany; wbensch@ac.uni-kiel.de

ABSTRACT

Applying identical amounts of starting materials allowed the solvothermal preparation of two new polyoxoniobates by controlling the pH value of the reaction mixture. Stirring the slurries afforded crystallization of $K_5[Cu(H_2O)_2(cyclam)]_{1.5}\{[Cu(cyclam)][Cu(H_2O)(cyclam)]_2HSiNb_{18}O_{54}\}(NO_3)\cdot 30H_2O$ (**I**) and $\{[Cu(cyclam)(H_2O)]_2[Cu(cyclam)][Nb_{10}O_{28}]\}_n\cdot 9nH_2O$ (**II**) within short reaction times and in high yields. While compound **I** crystallizes from the mother liquor at room temperature after hydrothermal treatment at pH values > 10.3, compound **II** is isolated at pH < 10.3 by filtration, i.e **II** is formed at the reaction conditions applied. Time-dependent experiments demonstrate that under stirring, pure samples of both compounds can be obtained within 30 min. Syntheses without stirring the educt mixtures leads to very low yields of **I** and crystallization of **II** in comparable yields afforded about 20 h reaction time. In the structure of **I**, the rare $[SiNb_{18}O_{54}]^{14-}$ anion is found, which is surrounded by $[Cu(cyclam)]^{2+}$ complexes and K^+ cations. The water molecules form a very unusual hydrogen bonding pattern which may be classified as a

L4(2)4(4)5(4)10(4)16(6)42(14) water cluster. Compound **II** features the decaniobate anion $[Nb_{10}O_{28}]^{6-}$, is obtained after short reaction time in high yields and exhibits a reversible release/uptake of crystal water molecules.

INTRODUCTION

High nuclearity polyoxometalates (POMs) with cluster shells of different shape, charge and functionalities form an outstanding class of materials with enormous structural varieties and applications in various fields like medicine and catalysis[1–12]. While high-nuclearity POM clusters based on Mo or W crystallize in a wide pH range between approx. 0 and 8.5[13–19,20], the product formation among group V POMs is more sensitive to changes of the pH value[21–24]. In contrast to molybdates and tungstates, where a great variety of precursors like e.g. $[MoO_4]^{2-}$, $[WO_4]^{2-}$, $\{Mo_7O_{24}\}$, $\{PW_{12}O_{40}\}$ or $\{P_2W_{18}O_{64}\}$ is available, the number of suitable starting materials containing pre-built cluster shells in the field of polyoxovanadates (POVs) and polyoxoniobates (PONbs) is limited. The usage of heteroatom containing POVs as synthons was recently identified as a promising approach for the generation of new POVs[23,25], but such preformed compounds do not exist in the field of PONbs[24,26,27].

The niobium sources for preparation of PONbs are scarce: Nb_2O_5 is practically insoluble in common solvents and only reacts in alkaline melts to form a hexaniobate anion, while niobium alkoxide precursors like e.g. $Nb(OC_2H_5)_5$ are sensitive to air and moisture[24,28]. The resulting hydrolysis product $Nb_2O_5{\cdot}xH_2O$[29] can be dissolved in alkali or TMA^+ (tetramethylammonium) hydroxide solutions[30]. Among others, several Keggin ion derivatives like, e.g., $\{XNb_{12}O_{40-44}\}$ (X = Si[31,32,33,34], Ge[32,33], PV_2[35], V_3[36] PSb_2[37], PNb_2[37]) as well as Lindqvist type PONbs $\{H_xNb_6O_{19}\}$[38–41] (x = 0 - 4) could be crystallized using $Nb_2O_5{\cdot}xH_2O$ as niobium source.

One of the first PONb cluster geometries different from the prominent Lindqvist ion was the decaniobate anion $[Nb_{10}O_{28}]^{8-}$ (abbreviated as $\{Nb_{10}O_{28}\}$) composed of ten edge-sharing NbO_6 octahedra, which crystallized from an alkaline methanolic solution of niobium ethoxide ($Nb(OC_2H_5)_5$) after 24 h[42]. Due to the low stability of the alkoxide precursor, the syntheses were difficult to be reproduced[28], but this can be enhanced by employing directly $Nb_2O_5 \cdot xH_2O$[29]. The first TM amine complex (TM = transition metal) expanded $\{Nb_{10}O_{28}\}$ cluster was synthesized under hydrothermal conditions applying $K_7HNb_6O_{19} \cdot 13H_2O$[43]. Charge balance was achieved by *in-situ* generated $[TM(2,2'\text{-bipy})_2]^{2+}$ complexes (2,2′-bipy = 2,2′-bipyridine; TM = Co^{2+}, Zn^{2+}), which connect the anions via O-TM-O bridges into zigzag chains. With a similar synthesis protocol but at elevated temperatures, two decaniobate compounds of different dimensionalities (0D, 1D) were obtained containing $[Ni(2,2'\text{-bipy})_x]^{2+}$ (x = 2,3) complexes . In addition, decaniobates were also reported containing $[TM(1,10\text{-phen})_x]^{2+}$ complexes (TM = Ni^{2+}, Co^{2+}, Zn^{2+}; x = 2,3; 1,10-phen = 1,10-phenanthroline)[44].

Hydrothermal treatment of $[Nb_6O_{19}]^{8-}$ salts can also provide an avenue to cluster geometries which are unprecedented in PONb chemistry. In the presence of sodium metasilicate a new cluster geometry was prepared featuring the C-shaped $[SiNb_{18}O_{54}]^{14-}$ polyanion consisting of two full and two "half" hexaniobate subunits which encapsulate a $[SiO_4]^{4-}$ tetrahedron[45]. The $[SiNb_{18}O_{54}]^{14-}$ polyanion (abbreviated as $\{SiNb_{18}O_{54}\}$) could be isolated by a combination of hydrothermal and solvent diffusion methods. The latter was crucial for the formation of solid products, since clear solutions were obtained after hydrothermal treatments and solvent evaporation led only to gel-like phases. During further solvothermal syntheses, the first $\{SiNb_{18}O_{54}\}$ based inorganic-organic hybrid sample with composition $[Cu(en)_2]_3\{[Cu(en)_2][H_6SiNb_{18}O_{54}]\} \cdot 22H_2O$ (en = ethylenediamine) was synthesized[46]. The

polyanion could be also prepared with other main group elements as heteroatoms. Recently, the hydrothermal reaction between $\{Nb_6O_{19}\}$ and a monolacunary $\{GeW_{11}O_{39}\}$ Keggin-type ion led to the formation of $H[Cu(en)_2(H_2O)]_8[Cu(en)_2(H_2O)_2]_2\{K_4[Cu(en)_2]_2[Cu(en)_2(GeNb_{18}O_{54})]_2\}$-$[Nb_3W_3O_{19}]\cdot 32H_2O$, which represents a very interesting structure containing both C-shaped $\{GeNb_{18}O_{54}\}$ and Lindqvist $\{Nb_3W_3O_{19}\}$ moieties[47].

Although the solvothermal approach is powerful for synthesizing new and fascinating materials, the products cannot be predicted[48]. Most compounds were obtained by a trial-and-error method varying systematically different reaction parameters. Because of their chemical inertness and porous surface which benefits the growth of single crystals, Teflon lined steel autoclaves are widely used. But the usage of this experimental setup prevents visual control of the reaction progress and the reaction slurry cannot be stirred generating concentration gradients often leading to inhomogeneous products.

Applying dynamic hydrothermal conditions in glass tubes the two new compounds $K_5[Cu(H_2O)_2(cyclam)]_{1.5}\{[Cu(cyclam)][Cu(H_2O)(cyclam)]_2HSiNb_{18}O_{54}\}(NO_3)\cdot 30H_2O$ (**I**) and $\{[Cu(cyclam)(H_2O)]_2[Cu(cyclam)][Nb_{10}O_{28}]\}_n\cdot 9nH_2O$ (cyclam = 1,4,8,11-tetraazacyclotetradecane) (**II**) were prepared under identical conditions by adjusting the pH value. The structures are unique because a macrocyclic amine molecule could be successfully integrated in the PONb structure. Compound **I** is a rare example of an organic-inorganic hybrid based on the $[SiNb_{18}O_{54}]^{14-}$ anion and crystallizes after a short reaction time. In addition, compared to other known decaniobates, compound **II** could be obtained reproducibly in high yields within a very short reaction time of only 30 min. Compound **II** can be reversibly dehydrated and rehydrated without significantly affecting the crystallinity. Herein, we report the syntheses and characterizations of the two new compounds featuring two different PONb cores.

EXPERIMENTAL SECTION

Characterization techniques

X-ray powder patterns were recorded with Cu-Kα_1 radiation (λ = 1.540598 Å, Ge monochromator) on a STOE Stadi-P diffractometer with a Ge monochromator and a Mythen 1K detector. A Bruker Alpha-P IR spectrometer was used for measuring MIR spectra in a range of 4000 – 400 cm^{-1}. UV/Vis diffuse reflectance spectra were collected on an UV/Vis two-channel spectrometer Cary 5 from Carian Techtron Pty., Darmstadt, using $BaSO_4$ as white standard. Optical band gaps were estimated applying the Kubelka-Munk method[49]. CHN analyses were done with a EURO EA elemental analyzer (EURO VEKTOR). DTA-TG curves were measured under an air or nitrogen atmosphere on a Netzsch STA 409 CD with a heating rate of 4 K min^{-1}. DSC curves were recorded on a DSC Star System with STARe Excellence software (Mettler-Toledo AG) under air and nitrogen atmosphere. The calibration of the instruments was done using standard reference materials. Water sorption measurements were performed using a $Belsorp_{max}$ instrument (BEL JAPAN INC.) at 303 K. To remove the crystal water molecules the samples were treated in two different ways prior to the measurements: one sample was placed in an ampoule which was evacuated for 12 h at room temperature; the second sample was heated to 200 °C in N_2 atmosphere. Energy dispersive X-ray analyses (EDX) were done on a Philips Environmental Scanning Electron Microscope ESEM XL30 with an EDX detector. For structure determination the intensity data collection for both compounds was performed at 170 K with a STOE Imaging Plate Diffraction System (IPDS-2) with Mo-K_α radiation (λ = 0.71073 Å). The structures were solved with SHELXT-97[50] and refined against F^2 using SHELXL-2014[51]. For both compounds, a numerical absorption correction was performed (Tmin/max: 0.5409/0.7507

for **I** and 0.6261/0.7543 for **II**). All non-hydrogen atoms except some water O atoms in **II** were refined anisotropically. The C-H and N-H H atoms were positioned with idealized geometry and refined isotropically with U_{iso} (H) = 1.2 U_{eq} (C,N) using a riding model. In compound **I**, the water H atoms were not located but considered in the calculation of the molecular formula and the molecular weight. In total, 35 H_2O molecules were found. 32 of the oxygen positions are fully occupied, two are half occupied (O96, O98), and two further water O atoms are disordered with an occupancy of 80:20 (O76) and 70:30 (O97). The O-H H atoms in **II** were located in difference Fourier maps, and their bond lengths were set to ideal values and finally they were refined isotropically with U_{iso}(H) = 1.5 U_{eq}(O) using a riding model. After the structure refinement of **II**, some additional residual electron density peaks were observed in the difference Fourier map that indicate the presence of water molecules. Because no reasonable structure model was found the data were corrected for disordered solvents using the Squeeze option in Platon[52]. The residual number of electrons collected during the Squeeze procedure is 188, corresponding to five water molecules per formula unit. The solvent accessible free space calculated with Platon yields ~558 $Å^3$.

CCDC-1835027 (**I**) and CCDC-1835028 (**II**) contain the supplementary crystallographic data for this paper. These data can be obtained free charge from the Cambridge Crystallographic Data Centre via http://www.ccdc.cam.ac.uk/data_request/cif.

Syntheses

General: All chemicals except $K_7HNb_6O_{19}\cdot 13H_2O$ were purchased (Nb_2O_5: abcr, 99.5% Nb; $Cu(NO_3)_2\cdot 3H_2O$: Merck, >99 %, 1,4,8,11-tetraazacyclotetradecane: Alfa Aesar, >98 %, KOH, 85 %: abcr, HCl, 37 %: VWR) and were used without further purification. $K_7HNb_6O_{19}\cdot 13H_2O$ was synthesized applying a literature method[53]. The pH was adjusted with aqueous solutions of

1 M KOH or 1 M HCl. Unless otherwise mentioned, the reactions were carried out under hydrothermal conditions with stirring of the slurries (magnetic stirrer) in DURAN® glass tubes with an inner volume of 11 mL. To interrupt the reaction, the mixtures were quenched in ice-cold water after distinct time intervals of 30 min, 1 h, 2 h, etc. Subsequently, the solutions were filtered, transferred into straight glass tubes and the solvent was left to evaporate at room temperature. For comparison, some reactions were carried out without stirring in Teflon-lined steel autoclaves (inner volume: 30 mL) and the resulting solids were washed with water after separation by filtration.

$K_5[Cu(H_2O)_2(cyclam)]_{1.5}\{[Cu(cyclam)][Cu(H_2O)(cyclam)]_2HSiNb_{18}O_{54}\}(NO_3)$ $\cdot 30H_2O$ (I): 0.2 mmol $K_7HNb_6O_{19}\cdot 13H_2O$, 0.4 mmol $Cu(NO_3)_2\cdot 3H_2O$ and 0.4 mmol 1,4,8,11-tetraazacyclotetradecane (cyclam) were dispersed in 3 mL H_2O (pH = 12.3). The reaction mixture was kept under stirring at T = 130 °C for 3 h. The clear violet solution was transferred into a glass tube and after slow evaporation of the mother liquor violet block shaped crystals were obtained. Yield: 26 mg (6.4 % based on Nb). $C_{90}H_{358}N_{38}K_{10}Cu_9Si_2Nb_{36}O_{184}$: calcd. in %: C 11.65, H 3.89, N 5.73; found C 11.48, H 3.47, N 5.33.

$\{[Cu(cyclam)(H_2O)]_2[Cu(cyclam)][Nb_{10}O_{28}]\}_n\cdot 9nH_2O$ (II): *Method 1:* The same synthetic procedure was performed as for **I** but the pH was adjusted with 1 M aqueous HCl to < 10.4. During the reaction, a violet powder was formed. The microcrystalline solid product was recovered by filtration and was identified by PXRD as compound **II**. Yield: 72 mg at pH = 10.3 (26 % based on Nb). *Method 2:* Identical mixtures as in *method 1* were reacted in a Teflon-lined steel autoclave with an inner volume of 30 mL under static hydrothermal conditions. After 20 h at 130 °C, violet needles of **II** suitable for single crystal structure analysis were obtained. Yield:

120 mg (44 % based on Nb). $Cu_3C_{30}H_{94}N_{12}Nb_{10}O_{39}$: calcd. in %: C 15.22, H 4.00, N 7.10; found C 15.24, H 3.96, N 7.05.

RESULTS AND DISCUSSION

Synthetic Aspects

To the best of our knowledge, all literature-known PONbs synthesized *via* the hydrothermal route were obtained in Teflon-lined autoclaves. An interesting question is whether these materials crystallize before cooling the reactor and whether any intermediates are formed[24,48]. Beyond the lack of visual control, there are good reasons to replace the Teflon-liners as containers for hydrothermal syntheses. Due to the porous surface, Teflon can uptake small ions or molecules, which are difficult to remove and which may be released during the synthesis, impeding the reproducibility of the experiments. This is a disadvantage in particular for the preparation of PONbs, because their formation is very sensitive to changes of the reaction conditions[54]. Due to the possibility of visual control during the reaction, we used glass reactors and indeed, we observed the formation of one of the compounds presented here already during solvothermal treatment.

Stirring the reaction mixture (´dynamic´ conditions) leads to a homogeneous distribution of dissolved species and often phase pure products are formed. Under static conditions, single crystals are often obtained despite the unwanted concentration gradient in the slurry. We want to note that products of a dynamic reaction are not necessarily identical with those obtained from identical reaction mixtures without stirring[55].

We applied $K_7HNb_6O_{19}\cdot 13H_2O$ which is soluble in water and generates a pH value beneficial for formation of PONbs (pH ≈ 12). The *in-situ* generated $[Cu(cyclam)]^{2+}$ complex cation was

used because of the high stability[56] and the two vacant coordination sites which may lead to bond formation to O^{2-} anions of the PONb cluster.

For the synthesis of **I**, $K_7HNb_6O_{19}\cdot 13H_2O$, $Cu(NO)_3\cdot 3H_2O$ and cyclam were dissolved in water yielding a clear solution (Scheme 1) with a pH of ~12.3. After three hours, the solution was filtered, whereby no solid products were obtained. Slow evaporation of the mother liquor at room temperature to approx. 0.5 mL yielded $K_5[Cu(H_2O)_2(cyclam)]_{1.5}\{[Cu(cyclam)][Cu(H_2O)(cyclam)]_2HSiNb_{18}O_{54}\}(NO_3)\cdot 30H_2O$ (**I**) as violet block-shaped single crystals. Phase purity was confirmed by XRPD (Fig. S1).

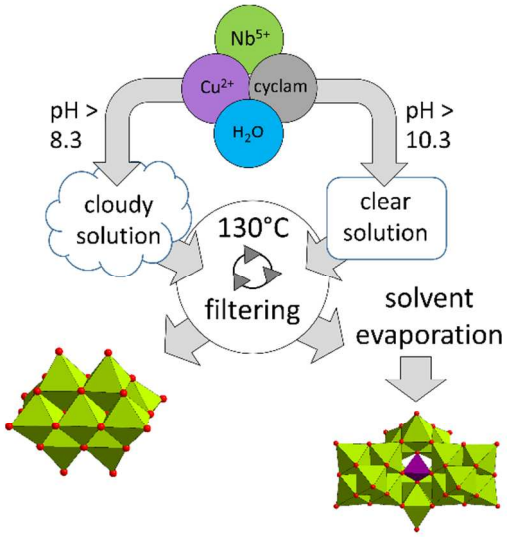

Scheme 1: Schematic representation of the syntheses of compounds **I** and **II**.

Time dependent syntheses demonstrated that the yield increased with prolongation of the reaction time. But even after 30 min. of reaction time, enough material crystallized from the mother liquor for XRPD characterization demonstrating phase purity of the product. The maximum yield could be obtained after 14 h (~43 %). In further experiments, the influence of the pH value onto product formation was investigated applying dynamic conditions. Prior to heating, the pH value of the reaction slurry was set between 8.3 and 10.3, whereby the formation of light

violet colored precipitates was observed. Reacting the mixtures at 130 °C the new compound $\{[Cu(cyclam)(H_2O)]_2[Cu(cyclam)][Nb_{10}O_{28}]\}_n \cdot 9nH_2O$ (**II**) was obtained as microcrystalline violet powder. In contrast to **I**, the formation of **II** could be optically observed during the reaction and the solid product that was recovered directly after filtration was identified as **II** by XRPD (Fig. S2). Evaporation of the mother liquor at room temperature did not afford further crystalline products. The yield was ~ 70 % (pH = 8.7) after 30 min. of reaction time, while no significant increase of the yield could be observed prolonging the time (after 3 h: 77 %). If the slurry is not stirred, the yield of **II** is reduced to ~2 % based on Nb after 30 min. This observation indicates that stirring achieves a more homogenous distribution of the reactants in solution. Interestingly, the yield of **II** decreases with increasing pH (~48% at pH = 9.5; ~26 % at pH = 10.3 for a reaction time of 3 h). This is in full accordance with reaction dynamics studies of aqueous solutions of $[Nb_{10}O_{28}]^{6-}$; where ^{17}O-NMR experiments in combination with ESI-MS revealed an increasing dissociation rate of decaniobate ions forming hexaniobate anions with increasing pH.[57]

Single crystal structure determination and EDX analysis of **I** clearly evidenced the presence of Si^{4+} ions, although no silicon source was employed in the reaction slurry. Hence, it must be assumed that alkaline pH leads to dissolution of silica from the glass tube. Repeating the synthesis in a Teflon-lined steel autoclave employing sodium metasilicate ($Na_2SiO_3 \cdot 3H_2O$) for 24 h at the same pH value of 12.3 without altering the remaining reaction parameters, compound **I** could be also obtained but in a very low yield. Therefore, we assume that the slow release of the silica species in the glass vessel benefits the crystallization of **I**. The incorporation of ions not supplied in the reaction slurry is not unprecedented and examples are $K_{14}Na[GaNb_{18}O_{54}] \cdot 31H_2O$[58] or in $K_{14}Na_6[H_4Ni_{10}(H_2O)_8Nb_{32}O_{102}] \cdot 73H_2O$[59] which were

synthesized without Na^+ cation supply or $K_{19}Na_4[H_{10}Nb_{31}O_{93}(CO_3)]\cdot 35H_2O$ which was formed by uptake of CO_2 from the atmosphere[54].

The study presented here validates the charge-density rule, which states that PONbs with higher charge densities are stable in a more alkaline pH regime[24,58]. The charge density is defined as the ratio between the charge of the anion and the number of non-hydrogen atoms.

According to this, **I** has a charge density of (13/73) = 0.178 and **II** (6/38) = 0.16. Because compound **I** was obtained at higher pH value, the system presented here follows this rule. Further prominent examples for the rule is the presence of $[Nb_6O_{19}]^{8-}$ at higher and $[Nb_{10}O_{28}]^{6-}$ at lower pH values (charge-densities: 0.32 and 0.16, respectively)[27,57].

Crystal Structures

$K_5[Cu(H_2O)_2(cyclam)]_{1.5}\{[Cu(cyclam)][Cu(H_2O)(cyclam)]_2HSiNb_{18}O_{54}\}(NO_3)\cdot 30H_2O$ (**I**)

crystallizes in the triclinic space group *P*-1 with one formula unit per unit cell with all atoms except one Cu^{2+} cation being located on general positions. Details of structure determination and refinement results are summarized in Tab. S1. The central structural motif consists of a $\{HSiNb_{18}O_{54}\}$ PONb cluster with three Cu^{2+} centered complexes attached covalently *via* terminal O atoms. The cluster shell (Fig. 1) contains two Lindqvist $\{Nb_6O_{19}\}$ structural units, two "half" Lindqvist groups $\{Nb_3O_{19}\}$ and a SiO_4 tetrahedron, which is connected by corner-sharing. Alternatively, the $\{Nb_3O_{19}\}$ triads and the SiO_4 tetrahedron may be viewed as a $\{SiNb_3O_{26}\}$ Keggin fragment, connected to two Lindqvist units *via* corner sharing.

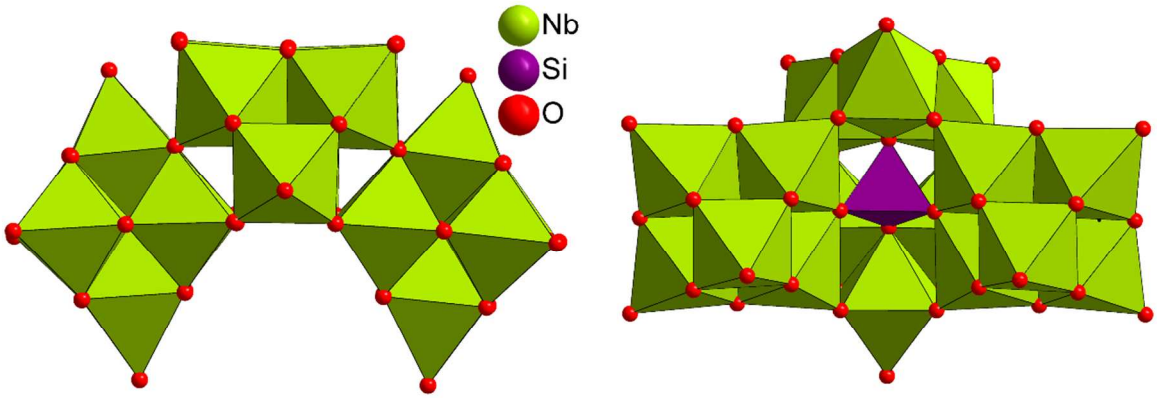

Figure 1. Different views on $\{HSiNb_{18}O_{54}\}$ PONb cluster; Green: NbO_6 octahedra; purple: SiO_4 tetrahedra. Attached Cu^{2+} centered complexes are not displayed.

In the $\{HSiNb_{18}O_{54}\}$ cluster, five different types of oxygen atoms can be identified: terminal $Nb{=}O_t$, Nb-μ_2-O, Si/Nb-μ_3-O, Si/Nb-μ_4-O and Nb-μ_6-O bridging atoms. The corresponding bond lengths are 1.739(5) - 1.770(5) Å, 1.811(5) - 2.076(5) Å, 1.639(4) - 2.235(4) Å, 1.626(4) - 2.491(4) Å and 2.209(4) - 2.546(4) Å, respectively (Tab. S2) and match well with values reported for $\{SiNb_{18}O_{54}\}$ containing compounds[45,46].

Bond valence sum calculations (BVS) yield an oxidation state of +5 for Nb with values ranging from 5.11 to 5.27 (average: 5.13, Tab. S3). The value for Si of 4.73 indicates an "over bonded" Si^{4+} ion, but the Si-O distances of 1.626(4) – 1.650(4) Å are in good agreement with those reported for other Si-PONbs[31,60]. Charge balance requires that the anion is monoprotonated. BVS calculations (Tab. S3) for O^{2-} anions provided values of 1.34 - 1.72 (average: 1.60) for terminal, 1.68 - 2.16 (average: 1.88) for μ_2-O and 1.93 - 2.09 (average: 1.99) for μ_3-O atoms, suggesting that most probably the proton is either located on O14 (BVS: 1.35) or delocalized over terminal O atoms.

The five crystallographically independent Cu^{2+} cations in the structure of **I** are coordinated by cyclam molecules and O atoms (Fig. 2).

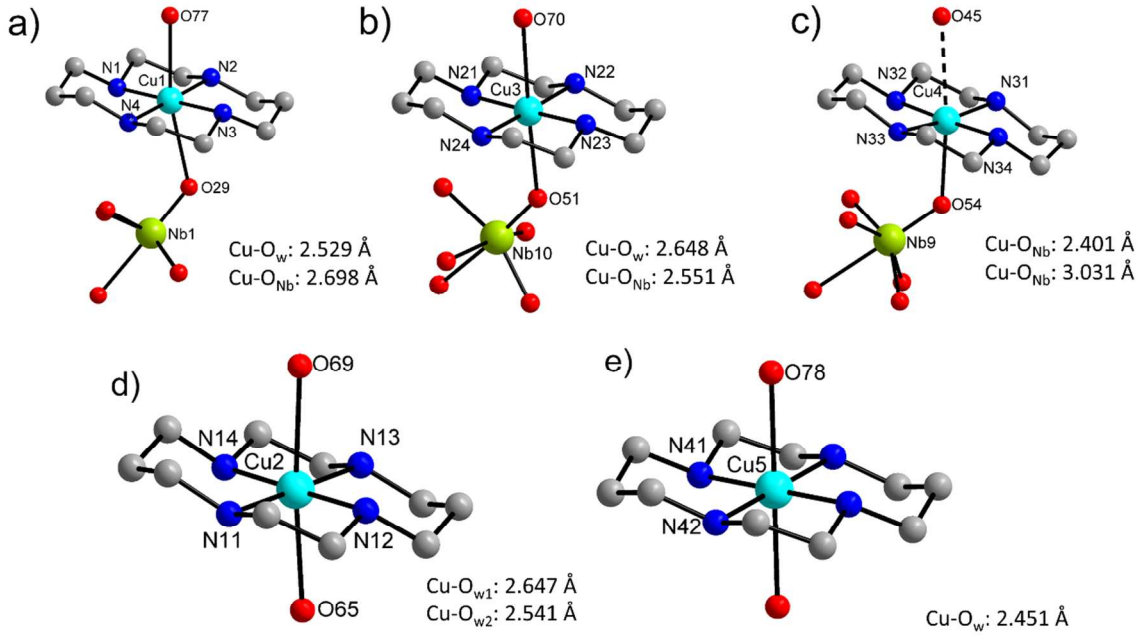

Figure 2a-e. View of the different coordination environments of the Cu^{2+} cations in the $[Cu(cyclam)]^{2+}$ complexes in **I** (O_W: water oxygen atoms, $O_{Nb:}$ terminal cluster oxygen atoms). H atoms are omitted for clarity. Besides the N atoms of the cyclam ligands in the equatorial plane, the octahedra are completed either by O atoms of water molecules (O_W) or both water O atoms and terminal O atoms of the cluster (O_{Nb}). The long Cu-O distance is shown in dashed lines.

Two Cu^{2+} cations (Cu1/ Cu3) are in an octahedral environment of four N atoms of the ligand, one O atom of a H_2O molecule and one terminal O atom of the cluster anion (Fig. 2a, b). Cu4 has bonds to the N atoms of one cyclam molecule and a terminal O atom of the anion yielding a distorted square pyramidal environment (Fig. 2c), while Cu2 and Cu5 are surrounded by one cyclam ligand and two H_2O molecules generating distorted octahedra (Fig. 2d, e). Cu4 has an O^{2-} anion of an adjacent cluster anion at 3.031(6) Å, but this distance is longer than the sum of the

van der Waals radii (2.92 Å[61]). The Cu-N bond lengths for all complexes scatter between 1.995(8) and 2.034(6) Å with N-Cu-N cis-angles between 85.1(3) and 94.9(3) ° and trans-angles of 173.8(3) - 180.0 ° (Tab. S4), in agreement with reported values[62–65]. The Cu-Ow (w = water) bonds are in the range of 2.451(8) - 2.648(6) Å and the latter is slightly longer than those reported for isolated copper cyclam complexes with aqua ligands with distances up to 2.531(2) Å[63,65–69] . The Cu-O bonds to terminal O2- anions of the cluster are between 2.401(6) and 2.698(4) Å. Such bond lengths were also observed in $[\{Cu(cyclam)\}(VO_3)_2]\cdot 5H_2O$[70]. Along [010] a chain-like arrangement is observed with alternating short and long Cu-O distances (Fig. 3). Overall, each anion is decorated by three Cu^{2+} centered complexes and the remaining two $[Cu(cyclam)(H_2O)]^{2+}$ molecules are located between the chain-like arrangement (Fig. S3 and S4).

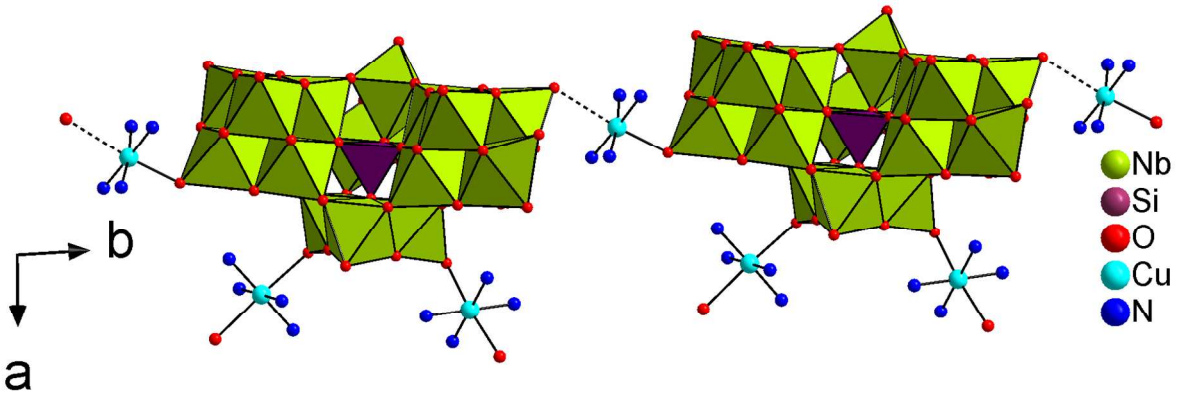

Figure 3. View of $\{HSiNb_{18}O_{54}\}$ clusters decorated by $[Cu(cyclam)(H_2O)]^{2+}$ and $[Cu(cyclam]^{2+}$ cations in the structure of **I**. Dotted line: long Cu-O distances (Cu(4)-O(45): 3.031(6) Å). Green polyhedra: NbO_6; purple polyhedra: SiO_4. Water O atoms, K^+ cations and NO_3^- anions as well as C and H atoms are not displayed for the sake of clarity.

Four of the five unique K^+ cations are located between two $\{HSiNb_{18}O_{54}\}$ clusters and one (K4) is found in the pocket of the cluster anion (Fig. 4).

Each potassium ion is surrounded by water molecules and cluster O^{2-} anions and have coordination numbers (CN) of 5 (K3), 6 (K4), 7(K1, K2) and 8 (K5) with average K-O bond lengths of 2.812 - 2.881 Å using a cutoff of 3.03 Å for the interionic distances. We note that the sum of ionic radii is 2.72 – 2.89 Å[71], depending on the CN. K3 is located in the plane of four O^{2-} anions, which is electrostatically not satisfiying. Therefore, K-O distances up to 3.15 Å were considered, which leads to an increase of the CN to 6 (K3), 8 (K1, K2, K5) and 9 (K4), respectively (Tab. S5, Fig. S5a). Such long K-O separations up to ~3.2 Å are not unusual and were already reported for $KOH{\cdot}4H_2O$[72] or in $K_{14}H[K@Si_4Nb_{16}O_{56}]{\cdot}26H_2O$[73].

The polyhedra around the K^+ cations are irregular and they share edges and corners e.g. the polyhedron around K3 shares corners with those around K1 and K5 (Fig. S5b). The KO_x polyhedra adopt an one-dimensional arrangement between the cluster anions along [010] (Fig. S6).

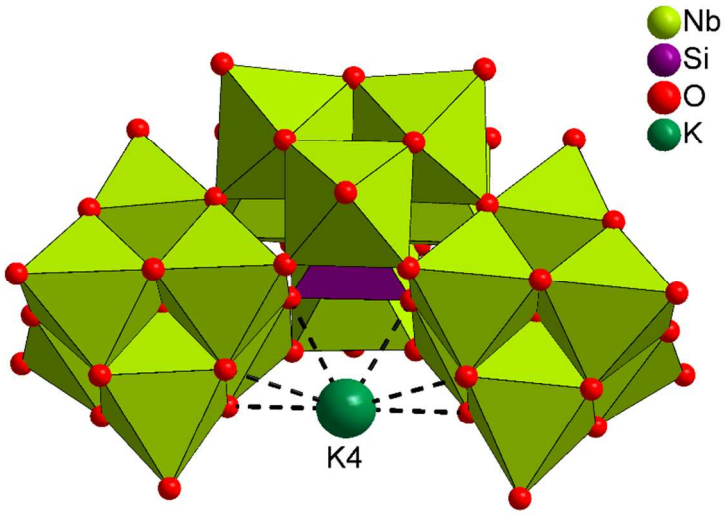

Figure 4. View of the $[HSiNb_{18}O_{54}]^{13-}$ anionic unit in **I**. The location of the K4 ion is displayed.

Because the H atoms of the 35 H_2O molecules could not be located, O···O distances up to the sum of the van der Waals radii (3.04 Å) were considered as possible donor-acceptor distances for O-H···O bonds. The O···O distances range from 2.616 to 2.987 Å (Tab. S6), and a complex pattern is generated in the bc plane containing H_2O bonded to Cu^{2+} cations and proposed H_2O molecules surrounding K+ cations. As mentioned above some H_2O are disordered and for sake of clarity these molecules are not considered. Following the notation of Infantes et al.[74,75] the water network can be denoted as L4(2)4(4)5(4)10(4)16(6)42(14), i.e. there are four-membered rings which are surrounded by two or four other rings, five-membered rings sharing H_2O molecules of four other rings, etc. (Fig. S7). In the 16-membered rings, the $[Cu(cyclam)(H_2O)_2]^{2+}$ cations are located, while each cavity in the 42-membered rings is occupied by two $\{HSiNb_{18}O_{54}\}$ clusters along [100] (Fig. 5). The view along [010] reveals that those rings are arranged in wave-like manner with the anions being located between the rings (Fig. S8). Some of the water molecules form 4-membered discrete water clusters that would be denoted as D3 and D4, respectively.

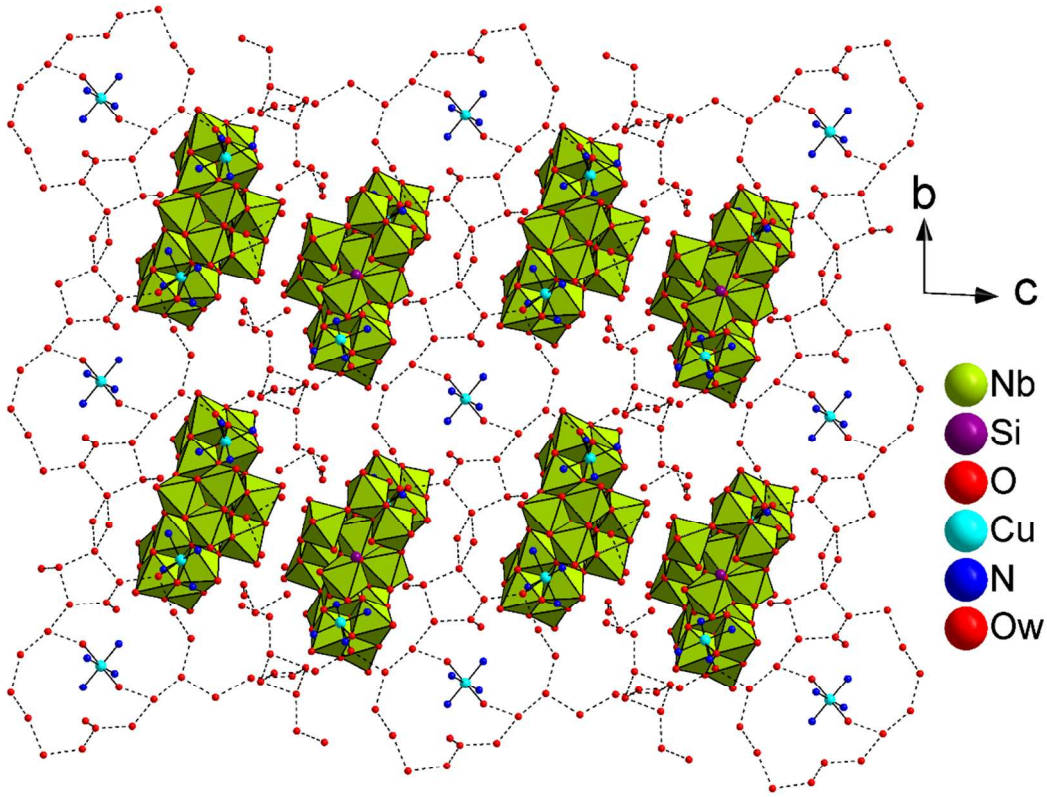

Fig. 5. View of the arrangement of the layered L4(2)4(4)5(4)10(4)16(6)42(14) water motif along [100] with the $\{SiNb_{18}O_{54}\}$ clusters located in the 42-membered rings in the structure of **I**. Green polyhedra: NbO_6; purple polyhedra: SiO_4; some atoms are omitted.

The compound $\{[Cu(cyclam)(H_2O)]_2[Cu(cyclam)][Nb_{10}O_{28}]\}_n \cdot 9nH_2O$ (**II**) crystallizes in the monoclinic space group C2/c (Table S1). All unique atoms except Cu2 are located on general positions. The two crystallographically independent Cu^{2+} cations are in a distorted octahedral coordination geometry with four N donors of the cyclam ligand in the equatorial plane and two O2- anions in axial positions. The orientation of the N-H protons of the cyclam molecules around both Cu1 and Cu2 yields the trans-III (S,S,R,R) configuration[56,76,77] (Fig. 6).

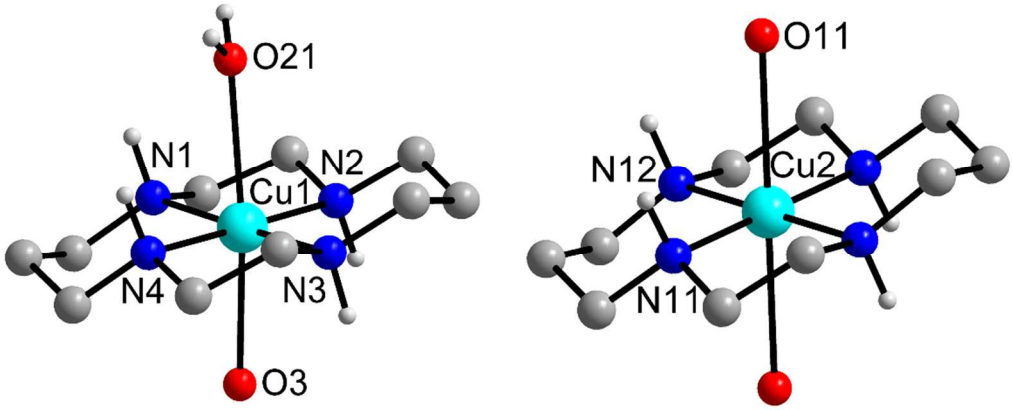

Figure 6. View of of the coordination environments around the two crystallographically independent Cu^{2+} cations in **II**. Only selected atoms are labelled. Ligand H atoms omitted.

All Nb centers are in an octahedral environment of O^{2-} anions and the NbO_6 octahedra are connected via edge-sharing to form the $\{Nb_{10}O_{28}\}$ decaniobate ion (Fig. 7). The geometry may be described as a rectangle generated by six edge-sharing NbO_6 octahedra which is capped by four NbO_6 units. The O^{2-} anions can be grouped according to the number of bridging metal atom centers: Nb-O_t, Nb-μ_2-O, Nb-μ_3-O and Nb-μ_6-O with bond lengths 1.738(3) - 1.753(3) Å, 1.916(3) - 2.097(3) Å, 2.009(3) – 2.138(3) Å and 2.225(2) - 2.545(2) Å, respectively (Tab. S7), agreeing with data reported for other decaniobate compounds[42–44,78]. The O-Nb-O angles scatter from 73.2(1) to 164.3(1) ° (Tab. S8) reflecting a pronounced distortion of the NbO_6 octahedra. BVS calculations confirm the oxidation state of +5 for all Nb centers (average: 5.05, Tab. S3).

The $[Nb_{10}O_{28}]^{6-}$ anion is decorated by two $[Cu(cyclam)(H_2O)]^{2+}$ molecules via Nb-O_t-Cu bonds (Fig. 7) involving ions which are the most basic sites of the decaniobate anion[57].

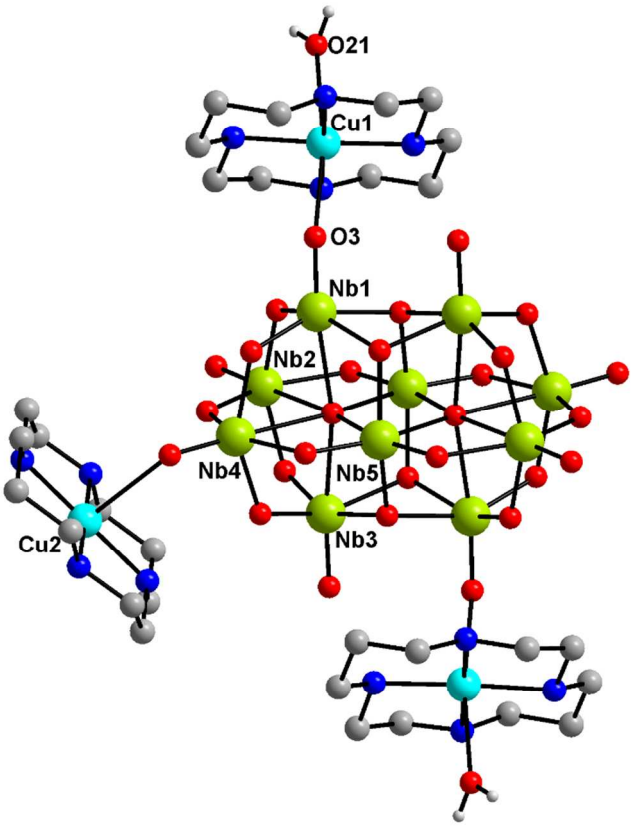

Figure 7. View of the decaniobate anion in **II**, decorated by three Cu^{2+} centered complexes.Only selected atoms are displayed and only a few atoms are labelled.

The corresponding Cu1-O3 and Cu2-O11 distances are 2.469(3) Å and 2.721(4) Å respectively connecting the $\{Nb_{10}O_{28}\}$ anions into a chain directed along [100] (Fig. 8).

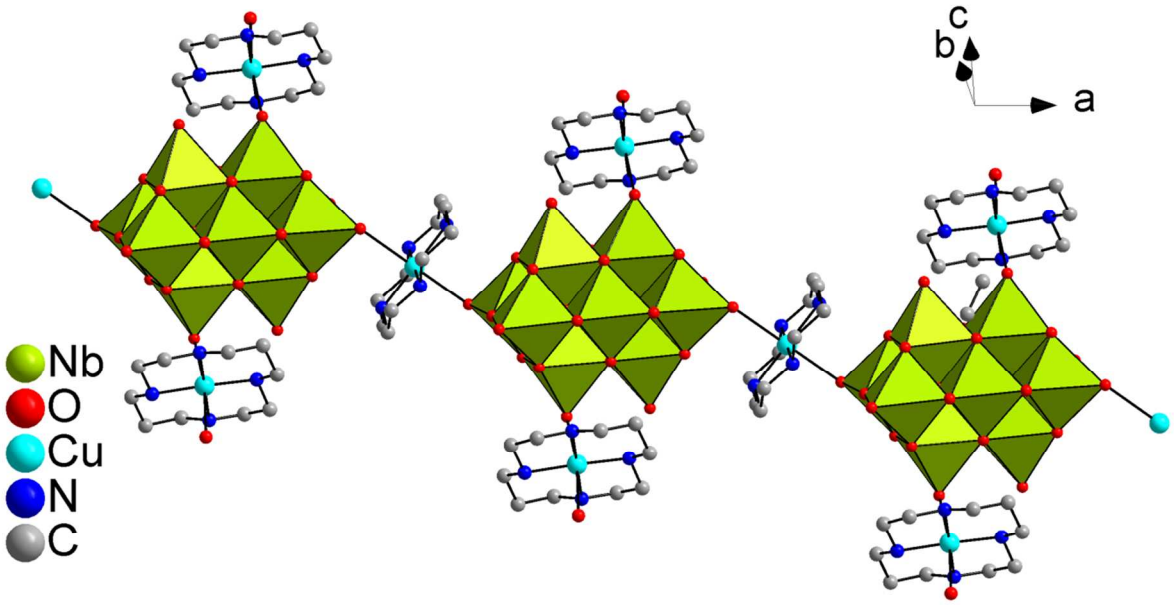

Figure 8. View of the chain generated through long Cu-O bonds in the structure of **II**. H atoms and crystal water molecules are omitted for clarity.Green polyhedra: NbO_6 units.

The Cu-O_w bond of 2.594(5) Å is only slightly longer than those reported for $[Cu(cyclam)]^{2+}$ complexes containing compounds[63,65–69]. The Cu-N bonds are between 2.005(3) and 2.030(4) Å with N-Cu-N angles of 85.6(2) and 94.6(2) ° (Tab. S9), in good accordance with data reported in literature[63,64,68,6968]. Concerning the N/O-Cu-N/O angles, the $[Cu(cyclam)(H_2O)]^{2+}$ complex is more distorted (81.2(2) - 172.1(1) °) than the other one (85.5(1) - 180 °). A possible reason is the involvement of the H_2O molecule in intramolecular H bonding interaction (N-H···O: 3.038(6) Å; < (NHO) = 111.6 °) and O-H···O interactions with O_t atoms of neighboring clusters (Fig. S9) (O-H···O: 2.746(5) Å; < (OHO) = 167.7 °). Hydrogen bonds between the H_2O ligand and terminal O atoms of the $[Nb_{10}O_{28}]^{6-}$ anion connect the clusters along the *c* axis (Fig. 9).

Strong hydrogen bonds (Tab. S10) are found between the N-H atoms of the cyclam ligands and the terminal and μ_2-bridging O atoms of the decaniobate anion (N-H···O distances: 2.949(4) –

3.049(4) Å; < (NHO) = 145.9 – 168.4 °). Furthermore, C-H atoms of cyclam and terminal as well as bridging (μ_2-, μ_3-O) cluster O^{2-} anions (C-H···O distances: 3.241(6) – 3.480(6) Å; < (CHO) = 123.6 ° - 158.3 °) are also involved in H bonding interactions. The crystal water molecules exhibit relatively strong H bonding interactions with terminal and μ_2-bridging cluster O^{2-} anions (O-H···O distances: 2.798(4) – 3.217(5) Å; < (OHO) = 139.1 ° - 175.4 °) and weaker interactions with the C-H H atoms of the cyclam molecule ((C-H···O distances: 3.258(6) – 3.579(7) Å; < (CHO) = 125.8 ° - 169.9 °). The two unique H_2O molecules form a cluster which can be denoted as D2 (D = discrete) following the nomenclature of Infantes *et al.* [74,75]. This D2 unit interacts with O^{2-} of the cluster anions via O-H···H bonds leading to a R4 motif (R = ring).

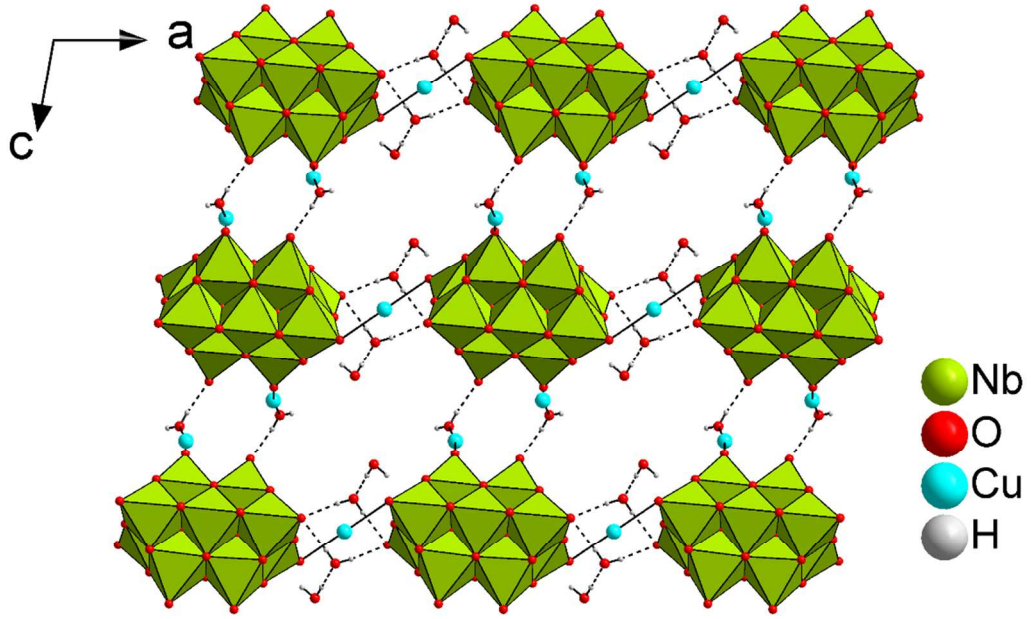

Figure 9. View of the arrangement of crystal water molecules in compound **II** and their involvement in hydrogen bonds (shown as dashed lines). Green polyhedra: NbO_6; organic ligands are omitted for clarity.

Optical properties in the UV-Vis region

To estimate the band gaps from UV-Vis data, the Kubelka-Munk relation was applied (Fig. S10 and S11). For **I**, the broad absorption at 519 nm (2.39 eV) arises from Cu^{2+} d-d transitions $E_g \rightarrow {}^2T_{2g}$ [79,80,81,82], while for **II**, the same transition occurs at 521 nm (2.38 eV). Both transitions correspond to the absorption of green light, in good accordance to the violet colour of the compounds. The strong absorption located at about 326 nm (3.8 eV) for both compounds is most probably a charge transfer band.

Thermal investigations

The thermal properties of both compounds were investigated in air and nitrogen atmosphere. Regardless of the atmosphere, compound **I** decomposes in not well-resolved steps (Fig. S12 and 13). When heated in an air, the first mass loss of about 15 %, which is accompanied by an endothermic event (T_p = 104 °C), matches well with the emission of 35 water molecules (calc. 14.9 %). Starting at ~ 200°C and up to 650 °C, further decomposition with a mass loss of about 20 % is observed, which may be explained by the emission of cyclam molecules (calc. 19.5 %). The reflections in the XRDP of the sample obtained at 500 °C could be assigned to Cu and CuO (Fig. S14a). We want to note that in the XRDP of several decomposition samples, modulated backgrounds are observed indicating the presence of X-ray amorphous material. Heating to 1000 °C a dark green residue is formed and most of the reflections in the XRDP could be assigned to $CuNb_2O_6$, $K_{5.75}Nb_{10.85}O_{30}$ and SiO_2 (Fig. S14b). Heating the sample to 1000° C in N_2, the TG curve above 200 °C is less steep compared to decomposition in air (Fig. S15). The residue recovered at 600 °C showed only reflections of CuO in the XRPD (Fig. S16a). The XRPD of the black powder formed at 1000 °C (Fig. S16b) exhibits a large number of reflections and an

unambiguous assignment to known compounds is difficult, but most of them could be assigned to $K_xNb_yO_{30}$ ($x \sim 6$, $y \sim 10.8$), Cu, NbO_2 and SiO_2.

In the TG curve of **II** measured in air, a well resolved mass loss up to ~ 200 °C with an endothermic event at T_p = 129 °C occurs which can be assigned to the loss of crystal water molecules (Fig. S17). During structure refinement, six H_2O molecules could be located. As mentioned above (See Experimental), five additional water molecules may occupy void spaces, giving rise to eleven H_2O molecules per formula unit. This is in full agreement with the first mass loss of 8.4 % (calc. 8.4 %). The following decomposition reaction from 200 - 500 °C (Δm = 23.2 %) is accompanied by three exothermic signals at T_p = 300, 349 and 365 °C as well as a broad shoulder around 400 °C, which is better resolved in the DSC curve (Fig. S18) with T_p = 396 °C. The mass loss between 200 and 600 °C of 26 % is in good agreement with removal of three cyclam molecules (calc. 25.2 %).When the decomposition is stopped at ~520 °C, an olive green solid containing ~ 1% residual C and N is obtained. The XRDP (Fig. S19a) revealed a modulated background and only two very weak reflections were observed, which may be assigned to CuO. The light green solid isolated after heating to 600 °C does not contain any residual C or N. The reflections in the powder pattern could not be assigned to any known copper or niobium or mixed oxides (Fig. S19b). Furthermore, the material seems to be nanocrystalline in nature. Further investigations concerning the composition and properties are under way. After heating to 1000 °C, the XRPD of the light green residue shows mainly reflections of $Nb_{12}O_{29}$ and $CuNb_2O_6$ (Fig. S19c).

The TG curve collected in N_2 atmosphere exhibits only two mass steps until ~600 °C (Fig. S20 and S21). The black residue at 600 °C contains elemental Cu (Fig. S22a), in contrast to the experiment carried out in air where an unidentified material was obtained. The decomposition is

not complete at 1000 °C and the sample still contains residual C (~5 %) and N (~1.3 %). Most reflections in the XRDP can be assigned to Cu and NbO_2 (Fig. S22b).

In contrast to **I**, a pronounced plateau is observed after removal of H_2O. In a further experiment, decomposition was stopped at 200 °C and the residue was investigated with PXRD. The material exhibits a good crystallinity after dehydration and the powder pattern clearly differs from the simulated pattern of **II** (Fig. S23). After stirring the dehydrated sample for 2 h in water and drying on air, the powder pattern matches well with the simulated pattern of **II**, indicating that the material is fully recovered (Fig. S24).

The water adsorption properties of **II** were investigated with water vapor sorption measurements using samples treated in different ways (see Experimental Section). The sorption isotherm of the sample dehydrated at room temperature by evacuation shows a water uptake of only ~ 7 of the 11 crystal water molecules at a partial pressure $p/p_0 = 0.9$ (Fig. 10). For the sample heated at 200 °C the uptake of 7 H_2O molecules is already reached at $p/p_0 = 0.7$ and a higher partial pressure is required for adsorption of all 11 molecules. The different behavior of the two samples can be traced back to the crystal structures: evacuation does not significantly change the crystal structure while heat treatment at 200 °C leads to formation of a new compound with a different crystal structure (Fig. S29).

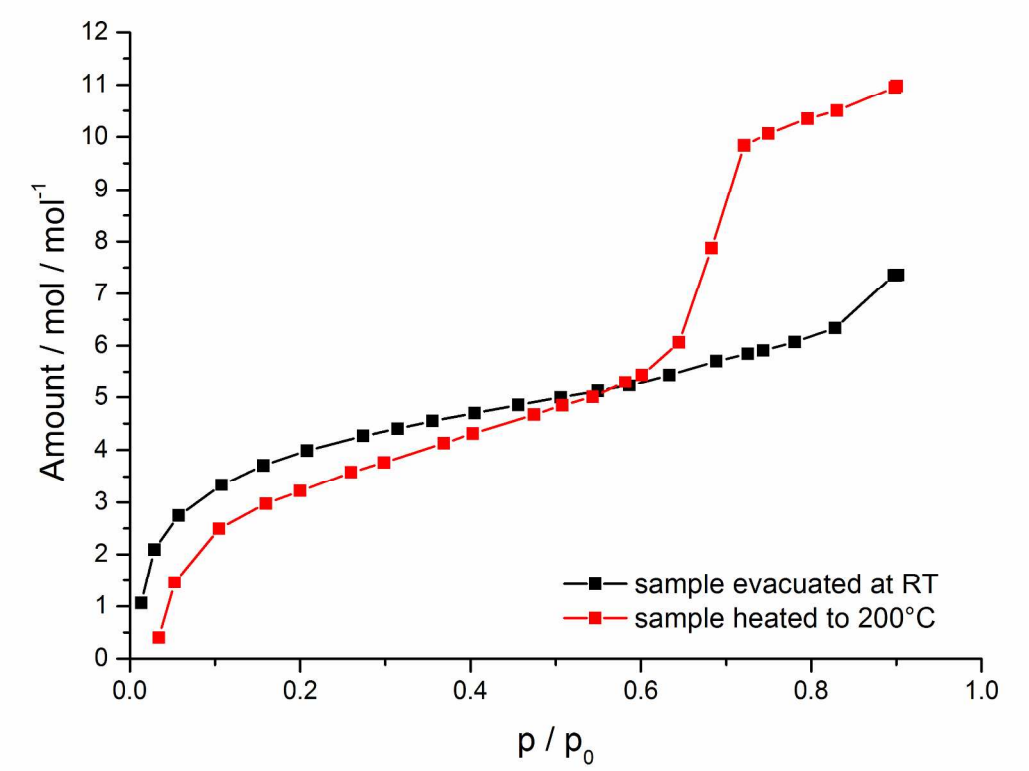

Figure 10. Water sorption isotherms of samples of compound **II** evacuated at room temperature (black) and heated to 200 °C (red).

CONCLUSION

We demonstrated that control of the pH value is an important synthetic parameter for the directed preparation of new polyoxoniobates. In addition the pH value significantly influences the yield of the compounds and also stirring the reaction slurry is required for formation of phase pure products. The rare $\{SiNb_{18}O_{54}\}$ cluster in the structure of **I** is covalently expanded by Cu^{2+}centered complexes. Crystal lattice water molecules form a complex network through H bonding interactions. In the structure of **II** decaniobate anions are connected into a chain *via* Cu-O_t bonds of $[Cu(cyclam)]^{2+}$ cations along [100]. Compound **I** is decomposed upon heating in several not well resolved steps, and depending on the atmosphere and final temperature different compounds are formed. The TG curve of **II** shows a distinct plateau due to removal of crystal

water molecules. The XRPD evidence that the dehydrated material exhibits good crystallinity and that **II** is recovered when treated with water. H_2O sorption measurements demonstrate that the water molecules can be desorbed *in vacuo* and confirm the number of water molecules determined from TG experiments and elemental analysis.

Because of the large potential of PONbs in various fields of possible applications, an efficient synthetic strategy with short reaction times and high yields is crucial to explore the potential of these new materials in a reasonable timescale. Because PONb based materials are often synthesized under hydrothermal conditions, systematic evaluations of the influence of a single reaction parameter onto product formation is necessary to understand the formation pathways. It is well documented that the products of hydrothermal syntheses are often inhomogeneous caused by concentration gradients in the reaction slurries. We demonstrated that phase pure products can be obtained stirring the reaction mixture which leads to a homogenous distribution of the reactants in solution. Furthermore, a shortening of the reaction time is advantageous for screening of the parameter space, thus allowing fast optimization of reaction parameters. Currently, we are systematically exploring if this approach is suitable for the efficient synthesis of new PONbs exhibiting new structural features and chemical compositions.

ASSOCIATED CONTENT

Supporting Information Additional tables with selected bond lengths and angles and bond valence sum analyses, images of the structures, powder patterns, DTA/TG curves of both compounds, DSC diagrams of compound **II**, IR spectra and assignments of the infrared absorption bands of both compounds, Kubelka-Munk plots.

AUTHOR INFORMATION

Corresponding Author

*E-mail: wbensch@ac.uni-kiel.de

Author Contributions

The manuscript was written through contributions of all authors. All authors have given approval to the final version of the manuscript.

ACKNOWLEDGMENT

The authors gratefully acknowledge financial support of the State Schleswig-Holstein and Lisa K. Mahnke for her help with the TOC graphic.

References

(1) Ogata, A.; Yanagie, H.; Ishikawa, E.; Morishita, Y.; Mitsui, S.; Yamashita, A.; Hasumi, K.; Takamoto, S.; Yamase, T.; Eriguchi, M. Antitumour effect of polyoxomolybdates: Induction of apoptotic cell death and autophagy in in vitro and in vivo models. *Br. J. Cancer* **2008**, *98*, 399–409.

(2) Mitsui, S.; Ogata, A.; Yanagie, H.; Kasano, H.; Hisa, T.; Yamase, T.; Eriguchi, M. Antitumor activity of polyoxomolybdate, $[NH_3Pr^i]_6[Mo_7O_{24}]\cdot 3H_2O$, against, human gastric cancer model. *Biomed. Pharmacother.* **2006**, *60*, 353–358.

(3) Long, D.-L.; Tsunashima, R.; Cronin, L. Polyoxometalates: Building Blocks for Functional Nanoscale Systems. *Angew. Chem. Int. Ed.* **2010**, *49*, 1736–1758.

(4) Thompson, K. Coordination chemistry of vanadium in metallopharmaceutical candidate compounds. *Coord. Chem. Rev.* **2001**, *219-221*, 1033–1053.

(5) Streb, C. New trends in polyoxometalate photoredox chemistry: From photosensitisation to water oxidation catalysis. *Dalton Trans.* **2012**, *41*, 1651–1659.

(6) Rao, K. V.; Rao, P.S.N.; Nagaraju, P.; Prasad, P. S.; Lingaiah, N. Room temperature selective oxidation of toluene over vanadium substituted polyoxometalate catalysts. *J. Mol. Catal. A. Chem.* **2009**, *303*, 84–89.

(7) Hill, C. L. Progress and challenges in polyoxometalate-based catalysis and catalytic materials chemistry. *J. Mol. Catal. A. Chem.* **2007**, *262*, 2–6.

(8) Han, X.-B.; Zhang, Z.-M.; Zhang, T.; Li, Y.-G.; Lin, W.; You, W.; Su, Z.-M.; Wang, E.-B. Polyoxometalate-Based Cobalt-Phosphate Molecular Catalysts for Visible Light-Driven Water Oxidation. *J. Am. Chem. Soc.* **2014**, *136*, 5359–5366.

(9) Dianat, S.; Bordbar, A. K.; Tangestaninejad, S.; Yadollahi, B.; Zarkesh-Esfahani, S. H.; Habibi, P. ctDNA binding affinity and in vitro antitumor activity of three Keggin type polyoxotungestates. *J. Photochem. Photobiol. A* **2013**, *124*, 27–33.

(10) Kozhevnikov, I. V. Catalysis by Heteropoly Acids and Multicomponent Polyoxometalates in Liquid-Phase Reactions. *Chem. Rev.* **1998**, *98*, 171–198.
(11) Katsoulis, D. E. A Survey of Applications of Polyoxometalates. *Chem. Rev.* **1998**, *98*, 359–388.
(12) Ji, Y.; Huang, L.; Hu, J.; Streb, C.; Song, Y.-F. Polyoxometalate-functionalized nanocarbon materials for energy conversion, energy storage and sensor systems. *Energy Environ. Sci.* **2015**, *8*, 776–789.
(13) Yu, F.; Kong, X.-J.; Zheng, Y.-Y.; Ren, Y.-P.; Long, L.-S.; Huang, R.-B.; Zheng, L.-S. pH-dependent assembly of 0D to 3D Keggin-based coordination polymers: Structures and catalytic properties: Structures and catalytic properties. *Dalton Trans.* **2009**, 9503–9509.
(14) Yang, H.; Gao, S.; Lü, J.; Xu, B.; Lin, J.; Cao, R. pH-Dependent Syntheses and Crystal Structures of a Series of Organic-Inorganic Hybrids Constructed from Keggin or Wells-Dawson Polyoxometalates and Silver Coordination Compounds. *Inorg. Chem.* **2010**, *49*, 736–744.
(15) Sha, J.-Q.; Sun, J.-W.; Wang, C.; Li, G.-M.; Yan, P.-F.; Li, M.-T. Syntheses Study of Keggin POM Supporting MOFs System. *Cryst. Growth Des.* **2012**, *12*, 2242–2250.
(16) Li, S.; Zhang, L.; Chai, D.; Pang, H.; Ma, H. Self-assembly of polyoxometalate-based hybrid aggregates: From a monomer to dimers by changing the pH value of reaction systems. *New J. Chem.* **2017**, *41*, 10148–10154.
(17) Li, S.; Ma, H.; Pang, H.; Zhang, L. Assembly of Six Polyoxometalate-Based Hybrid Compounds from a Simple Supramolecule to a Complicated Pseudorotaxane Framework via Tuning the pH of the Reaction Systems. *Cryst. Growth Des.* **2014**, *14*, 4450–4460.
(18) Hu, Y.; An, H.; Liu, X.; Yin, J.; Wang, H.; Zhang, H.; Wang, L. pH-controlled assembly of hybrid architectures based on Anderson-type polyoxometalates and silver coordination units. *Dalton Trans.* **2014**, *43*, 2488–2498.
(19) Chi, Y.-N.; Cui, F.-Y.; Jia, A.-R.; Ma, X.-Y.; Hu, C.-W. pH-Dependent syntheses of copper–quinoxaline–polyoxotungstate hybrids: Variable role of Keggin-type polyanion in different pH conditions. *CrystEngComm* **2012**, *14*, 3183–3188.
(20) Li, F.; Xu, L. Coordination assemblies of polyoxomolybdate cluster framework: From labile building blocks to stable functional materials. *Dalton Trans.* **2011**, *40*, 4024–4034.
(21) Wu, H.-L.; Zhang, Z.-M.; Li, Y.-G.; Wang, X.-L.; Wang, E.-B. Recent progress in polyoxoniobates decorated and stabilized *via* transition metal cations or clusters. *CrystEngComm* **2015**, *17*, 6261–6268.
(22) Molina, P. I.; Sures, D. J.; Miró, P.; Zakharov, L. N.; Nyman, M. Bridging the opposite chemistries of tantalum and tungsten polyoxometalates. *Dalton Trans.* **2015**, *44*, 15813–15822.
(23) Wendt, M.; Näther, C.; Bensch, W. High Nuclearity Antimonato-Polyoxovanadate Cluster $\{V_{15}Sb_6O_{42}\}$ as a Synthon for the Solvothermal in situ Generation of α- and β-$\{V_{14}Sb_8O_{42}\}$ Isomers. *Chem. Eur. J.* **2016**, *22*, 7747–7751.
(24) Nyman, M. Polyoxoniobate chemistry in the 21st century. *Dalton Trans.* **2011**, *40*, 8049–8058.
(25) Wendt, M.; Mahnke, L. K.; Heidenreich, N.; Bensch, W. Nucleation and Crystal Growth of a $\{V_{14}Sb_8O_{42}\}$ Cluster from a $\{V_{15}Sb_6O_{42}\}$ Polyoxovanadate: In Situ XRD Studies. *Eur. J. Inorg. Chem.* **2016**, *2016*, 5393–5398.
(26) Bontchev, R. P.; Nyman, M. Evolution of polyoxoniobate cluster anions. *Angew. Chem., Int. Ed.* **2006**, *45*, 6670–6672.
(27) Nyman, M.; Burns, P. C. A comprehensive comparison of transition-metal and actinyl polyoxometalates. *Chem. Soc. Rev.* **2012**, *41*, 7354–7367.

(28) Nyman, M.; Criscenti, L. J.; Bonhomme, F.; Rodriguez, M. A.; Cygan, R. T. Synthesis, structure, and molecular modeling of a titanoniobate isopolyanion. *J. Solid State Chem.* **2003**, *176*, 111–119.
(29) Ohlin, C. A.; Villa, E. M.; Casey, W. H. One-pot synthesis of the decaniobate salt $[N(CH_3)_4]_6[Nb_{10}O_{28}] \cdot 6H_2O$ from hydrous niobium oxide. *Inorg. Chim. Acta* **2009**, *362*, 1391–1392.
(30) Anderson, T. M.; Alam, T. M.; Rodriguez, M. A.; Bixler, J. N.; Xu, W.; Parise, J. B.; Nyman, M. Cupric Siliconiobate. Synthesis and Solid-State Studies of a Pseudosandwich-Type Heteropolyanion. *Inorg. Chem.* **2008**, *47*, 7834–7839.
(31) Nyman, M.; Bonhomme, F.; Alam, T. M.; Rodriguez, M. A.; Cherry, B. R.; Krumhansl, J. L.; Nenoff, T. M.; Sattler, A. M. A General Synthetic Procedure for Heteropolyniobates. *Science* **2002**, *297*, 996–998.
(32) Bonhomme, F.; Larentzos, J. P.; Alam, T. M.; Maginn, E. J.; Nyman, M. Synthesis, Structural Characterization, and Molecular Modeling of Dodecaniobate Keggin Chain Materials. *Inorg. Chem.* **2005**, *44*, 1774–1785.
(33) Nyman, M.; Bonhomme, F.; Alam, T. M.; Parise, J. B.; Vaughan, Gavin M. B. $[SiNb_{12}O_{40}]^{16-}$ and $[GeNb_{12}O_{40}]^{16-}$: Highly Charged Keggin Ions with Sticky Surfaces. *Angew. Chem. Int. Ed.* **2004**, *43*, 2787–2792.
(34) Zhang, Z.; Lin, Q.; Kurunthu, D.; Wu, T.; Zuo, F.; Zheng, S.-T.; Bardeen, C. J.; Bu, X.; Feng, P. Synthesis and Photocatalytic Properties of a New Heteropolyoxoniobate compound: $K_{10}[Nb_2O_2(H_2O)_2][SiNb_{12}O_{40}] \cdot 12H_2O$. *J. Am. Chem. Soc.* **2011**, *133*, 6934–6937.
(35) Son, J.-H.; Ohlin, C. A.; Johnson, R. L.; Yu, P.; Casey, W. H. A Soluble Phosphorus-Centered Keggin Polyoxoniobate with Bicapping Vanadyl Groups. *Chem. Eur. J.* **2013**, *19*, 5191–5197.
(36) Son, J.-H.; Ohlin, C. Andre; Larson, E. C.; Yu, P.; Casey, W. H. Synthesis and Characterization of a Soluble Vanadium-Containing Keggin Polyoxoniobate by ESI-MS and ^{51}V NMR: $(TMA)_9[V_3Nb_{12}O_{42}] \cdot 18H_2O$. *Eur. J. Inorg. Chem.* **2013**, 1748–1753.
(37) Son, J.-H.; Casey, W. H. Reversible capping/uncapping of phosphorous-centered Keggin-type polyoxoniobate clusters. *Chem. Commun.* **2015**, *51*, 1436–1438.
(38) Y. Yuan, F. Li, X. Fu, P. Ma. Crystal Structure of a new 3D polyoxoniobate based on Lindqvist type polyoxoanion. *Huaxue Yanjiu* **2011**, 19–24.
(39) Fullmer, L. B.; Mansergh, R. H.; Zakharov, L. N.; Keszler, D. A.; Nyman, M. Nb_2O_5 and Ta_2O_5 Thin Films from Polyoxometalate Precursors: A Single Proton Makes a Difference. *Cryst. Growth Des.* **2015**, *15*, 3885–3892.
(40) Nyman, M.; Alam, T. M.; Bonhomme, F.; Rodriguez, M. A.; Frazer, C. S.; Welk, M. E. Solid-state Structures and Solution Behavior of Alkali Salts of the $[Nb_6O_{19}]^{8-}$ Lindqvist Ion. *J. Cluster Sci.* **2006**, *17*, 197–219.
(41) Alam, T. M.; Nyman, M.; Cherry, B. R.; Segall, J. M.; Lybarger, L. E. Multinuclear NMR Investigations of the Oxygen, Water, and Hydroxyl Environments in Sodium Hexaniobate. *J. Am. Chem. Soc.* **2004**, *126*, 5610–5620.
(42) Graeber, E. J.; Morosin, B. The Molecular Configuration of the Decaniobate Ion ($Nb_{10}O_{28}^{6-}$). *Acta Crystallogr. B.* **1977**, 2137–2143.
(43) Shen, L.; Li, C.-H.; Chi, Y.-N.; Hu, C.-W. $Zn(2,2'\text{-bipy})_2$/$Co(2,2'\text{-bipy})_2$ linked decaniobate $[Nb_{10}O_{28}]^{6-}$ clusters-zigzag neutral chains. *Inorg. Chem. Commun.* **2008**, *11*, 992–994.

(44) Niu, J.; Wang, G.; Zhao, J.; Sui, Y.; Ma, P.; Wang, J. Zero- or One-Dimensional Organic-Inorganic Hybrid Polyoxoniobates Constructed from Decaniobate Units and Transition-Metal Complexes. *Cryst. Growth Des.* **2011**, *11*, 1253–1261.
(45) Hou, Y.; Nyman, M.; Rodriguez, M. A. Soluble Heteropolyniobates from the Bottom of Group IA. *Angew. Chem.* **2011**, *123*, 12722–12725.
(46) Huang, P.; Qin, C.; Wang, X.-L.; Sun, C.-Y.; Xing, Y.; Wang, H.-N.; Shao, K.-Z.; Su, Z.-M. A new organic-inorganic hybrid based on the crescent-shaped polyoxoanion $[H_6SiNb_{18}O_{54}]^{8-}$ and copper-organic cations. *Dalton Trans.* **2012**, *41*, 6075–6077.
(47) Liu, B.-X.; Cai, Z.-W.; Yang, T.; Li, X.-X.; Yang, G.-Y.; Zheng, S.-T. A rare polyoxometalate based on mixed niobium-based polyoxoanions $[GeNb_{18}O_{54}]^{14-}$ and $[Nb_3W_3O_{19}]^{5-}$. *Inorg. Chem. Commun.* **2017**, *78*, 56–60.
(48) Pienack, N.; Bensch, W. In-situ Monitoring of the Formation of Crystalline Solids. *Angew. Chem. Int. Ed.* **2011**, *50*, 2014–2034.
(49) Kortüm, G.; Braun, W.; Herzog, G. Prinzip und Meßmethodik der diffusen Reflexionsspektroskopie. *Angew. Chem.* **1963**, *75*, 653–661.
(50) G.M. Sheldrick. *SHELXS-97: Program for the Solution of Crystal Structures*; University of Goettingen: Goettingen, 1997.
(51) G.M. Sheldrick. *SHELXL-2014: Program for the Refinement of Crystal Structures*; University of Goettingen: Goettingen, 2014.
(52) Spek, A. L. PLATON SQUEEZE. A tool for the calculation of the disordered solvent contribution to the calculated structure factors. *Acta Crystallogr. C* **2015**, *71*, 9–18.
(53) Filowitz, M.; Ho, R. K. C.; Klemperer, W. G.; Shum, W. Oxygen-17 nuclear magnetic resonance spectroscopy of polyoxometalates. 1. Sensitivity and resolution. *Inorg. Chem.* **1979**, *18*, 93–103.
(54) Tsunashima, R.; Long, D.-L.; Miras, H. N.; Gabb, D.; Pradeep, C. P.; Cronin, L. The Construction of High-Nuclearity Isopolyoxoniobates with Pentagonal Building Blocks: $[HNb_{27}O_{76}]^{16-}$ and $[H_{10}Nb_{31}O_{93}(CO_3)]^{23-}$. *Angew. Chem.* **2010**, *122*, 117–120.
(55) Hilbert, J.; Näther, C.; Bensch, W. Influence of the Synthesis Parameters onto Nucleation and Crystallization of Five New Tin-Sulfur Containing Compounds. *Inorg. Chem.* **2014**, *53*, 5619–5630.
(56) Fabbrizzi, L. A Lifetime Walk in the Realm of Cyclam. *Macrocyclic and Supramolecular Chemistry*; pp 165–199.
(57) Villa, E. M.; Ohlin, C. A.; Balogh, E.; Anderson, T. M.; Nyman, M.; Casey, W. H. Reaction Dynamics of the Decaniobate Ion $[HxNb_{10}O_{28}]^{(6-x)-}$ in Water. *Angew. Chem.* **2008**, *120*, 4922–4924.
(58) Hou, Y.; Alam, T. M.; Rodriguez, M. A.; Nyman, M. Aqueous compatibility of group IIIA monomers and Nb-polyoxoanions. *Chem. Commun.* **2012**, *48*, 6004–6006.
(59) Liang, Z.; Zhang, D.; Wang, H.; Ma, P.; Yang, Z.; Niu, J.; Wang, J. The $\{Ni_{10}Nb_{32}\}$ aggregate: a perspective on isopolyniobates as ligands. *Dalton Trans.* **2016**, *45*, 16173–16176.
(60) Zhang, Y.; Shen, J.-Q.; Zheng, L.-H.; Zhang, Z.-M.; Li, Y.-X.; Wang, E.-B. Four Polyoxonibate-Based Inorganic–Organic Hybrids Assembly from Bicapped Heteropolyoxonibate with Effective Antitumor Activity. *Cryst. Growth Des.* **2014**, *14*, 110–116.
(61) Bondi, A. van der Waals Volumes and Radii. *J. Phys. Chem. A* **1964**, *68*, 441–451.
(62) Pérez-Toro, I.; Domínguez-Martín, A.; Choquesillo-Lazarte, D.; Vílchez-Rodríguez, E.; González-Pérez, J. M.; Castiñeiras, A.; Niclós-Gutiérrez, J. Lights and shadows in the challenge

of binding acyclovir, a synthetic purine-like nucleoside with antiviral activity, at an apical-distal coordination site in copper(II)-polyamine chelates. *J. Inorg. Biochem.* **2015**, *148*, 84–92.
(63) Tajidi, N. S. A.; Abdullah, N.; Arifin, Z. Diaqua-(1,4,8,11-tetraazacyclotetradecane-$\kappa^4N^1,N^4,N^8,N^{11}$)copper(**II**) didodeca-noate dihydrate. *Acta Crystallogr. E* **2011**, *67*, m588-9.
(64) P. A. Tasker, L. Sklar. Crystal and molecular structure of di(perchlorato)(1,4,8,11-tetraazacyclotetradecane)copper(II). Cu(cyclam)$(ClO_4)_2$. *J. Cryst. Mol. Struct.* **1975**, 329–344.
(65) Tajidi, N. S. A.; Abdullah, N.; Arifin, Z.; Tan, K. W.; Ng, S. W. Diaqua-(1,4,8,11-tetraazacyclotetradecane-$\kappa^4N^1,N^4,N^8,N^{11}$)copper(**II**) bis-(4-methyl-benzoate) monohydrate. *Acta Crystallogr. E* **2010**, *66*, m890.
(66) John Emsley, M. A. Hydrogen bonds between free fluoride ions and water molecules: two x-ray structures. *J. Mol. Struct.* **1990**, 1–12.
(67) Tajidi, N. S. A.; Norbani, A.; Zainudin, A.; Kong, W. T.; Ng, S. W. Diaqua-(1,4,8,11-tetraazacyclotetradecane-$\kappa^4N^1,N^4,N^8,N^{11}$)copper(**II**)bis-(2,3,4,5,6-penta-fluoro-benzoate) dihydrate. *Acta Crystallogr. E* **2010**, *66*, m889.
(68) Tajidi, N. S. A.; Abdullah, N.; Arifin, Z.; Tan, K. W.; Ng, S. W. Diaqua-(1,4,8,11-tetraazacyclotetradecane-$\kappa^4N^1,N^4,N^8,N^{11}$)copper(**II**) dihepta-noate dihydrate. *Acta Crystallogr. E* **2010**, *66*, m887.
(69) Tajidi, N. S. A.; Abdullah, N.; Arifin, Z.; Tan, K. W.; Ng, S. W. Diaqua-(1,4,8,11-tetraazacyclotetradecane-$\kappa^4N^1,N^4,N^8,N^{11}$)copper(**II**) dideca-noate dihydrate. *Acta Crystallogr. E* **2010**, *66*, m888.
(70) Martín-Caballero, J.; Wéry, Ana San José; Artetxe, B.; Reinoso, S.; Felices, L. S.; Vilas, J. L.; Gutiérrez-Zorrilla, J. M. Sequential single-crystal-to-single-crystal transformations promoted by gradual thermal dehydration in a porous metavanadate hybrid. *CrystEngComm* **2015**, *17*, 8915–8925.
(71) Shannon, R. D. Revised Effective Ionic Radii and Systematic Studies of Interatomic Distances in Halides and Chalcogenides. *Acta Crystallogr. A.* **1976**, *32*, 751–767.
(72) Rütter, H.; Mootz, D. Hydrate schwacher und starker Basen. V. Die Kristallstrukturen von KOH · $2H_2O$ (Substruktur) und KOH · $4H_2O$. *Z. Anorg. Allg. Chem.* **1991**, 73–82.
(73) Abramov, P. A.; Davletgildeeva, A. T.; Sokolov, M. N. Formation of Silicon-Containing Polyoxoniobates from Hexaniobate Under High Temperature Conditions. *J. Cluster Sci.* **2017**, *28*, 735–744.
(74) Infantes, L.; Chisholm, J.; Motherwell, S. Extended motifs from water and chemical functional groups in organic molecular crystals. *CrystEngComm* **2003**, *5*, 480–486.
(75) Infantes, L.; Motherwell, S. Water clusters in organic molecular crystals. *CrystEngComm* **2002**, *4*, 454–461.
(76) Bakaj, M.; Zimmer, M. Conformational analysis of copper(II) 1,4,8,11-tetraazacyclotetradecane macrocyclic systems. *J. Mol. Struct.* **1999**, *508*, 59–72.
(77) Kent Barefield, E. Coordination chemistry of N-tetraalkylated cyclam ligands—A status report. *Coord. Chem. Rev.* **2010**, *254*, 1607–1627.
(78) M. Matsumoto, Y. Ozawa, A. Yagasaki. Reversible dimerization of decaniobate. *Polyhedron* **2010**, 2196–2201.
(79) Boiocchi, M.; Broglia, A.; Fabbrizzi, L.; Fusco, N.; Mangano, C. Anion receptors containing coordinatively unsaturated metal ions: copper(II) complexes with cyclam derivatives. *Can. J. Chem.* **2014**, *92*, 794–802.
(80) Černák, J.; Kuchár, J.; Stolárová, M.; Kajňaková, M.; Vavra, M.; Potočňák, I.; Falvello, L. R.; Tomás, M. Preparation, spectroscopic and magnetic characterization of Cu(cyclam)$M(CN)_4$

complexes exhibiting one-dimensional crystal structures (cyclam = 1,4,8,11-tetraazacyclotetradecane, M = Ni, Pd, Pt). *Transit. Met. Chem.* **2010**, *35*, 737–744.

(81) Prevedello, A.; Bazzan, I.; Dalle Carbonare, N.; Giuliani, A.; Bhardwaj, S.; Africh, C.; Cepek, C.; Argazzi, R.; Bonchio, M.; Caramori, S. *et al.* Heterogeneous and Homogeneous Routes in Water Oxidation Catalysis Starting from Cu(II) Complexes with Tetraaza Macrocyclic Ligands. *Chem. Asian J.* **2016**, *11*, 1281–1287.

(82) Stephan, H.; Geipel, G.; Appelhans, D.; Bernhard, G.; Tabuani, D.; Komber, H.; Voit, B. Pegylation of 1,4,8,11-tetraazacyclotetradecane (cyclam) and its Cu(II) complexation. *Tetrahedron Lett.* **2005**, *46*, 3209–3212.

For Table of Content Use Only.

Controlling Fast Nucleation and Crystallization of Two New Polyoxoniobates

Joanna. Dopta, Dana-Céline Krause, Christian Näther, Wolfgang Bensch*

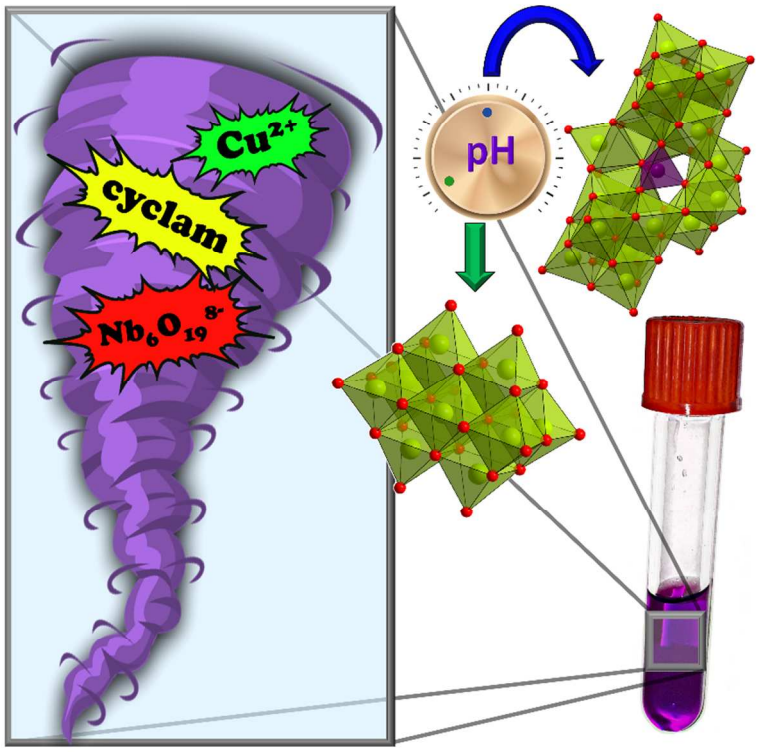

Two inorganic-organic polyoxoniobates $K_5[Cu(H_2O)_2(cyclam)]_{1.5}\{[Cu(cyclam)][Cu(H_2O)(cyclam)]_2HSiNb_{18}O_{54}\}(NO_3)\cdot 30H_2O$ (**I**) and $\{[Cu(cyclam)(H_2O)]_2[Cu(cyclam)][Nb_{10}O_{28}]\}_n\cdot 9nH_2O$ (**II**) were prepared from the same starting materials by altering the pH value of the reaction slurry.